Biophysical Journal Volume 89 December 2005 4111–4121

A Molecular Dynamics Study of the Response of Lipid Bilayers and Monolayers to Trehalose

Anna Skibinsky, Richard M. Venable, and Richard W. Pastor
Laboratory of Biophysics, Center for Biologics Evaluation and Research, Food and Drug Administration, Rockville, Maryland 20852-1448

ABSTRACT Surface tensions evaluated from molecular dynamics simulations of fully hydrated dipalmitoylphosphatidylcholine bilayers and monolayers at surface areas/lipid of 54, 64, and 80 Å^2 are uniformly lowered 4–8 dyn/cm upon addition of trehalose in a 1:2 trehalose/lipid ratio. Constant surface tension simulations of bilayers yield the complementary result: an increase in surface area consistent with the surface pressure-surface area (π-A) isotherms. Hydrogen bonding by trehalose, replacement of waters in the headgroup region, and modulation of the dipole potential are all similar in bilayers and monolayers at the same surface area. These results strongly support the assumption that experimental measurements on the interactions of surface active components such as trehalose with monolayers can yield quantitative insight to their effects on bilayers. The simulations also indicate that the 20–30 dyn/cm difference in surface tension of the bilayer leaflet and monolayer arises from differences in the chain regions, not the headgroup/water interfaces.

INTRODUCTION

The stabilizing effect of α,α-trehalose (Fig. 1) on lipid bilayers is well documented, but not well understood (1,2). To gain insight into how this disaccharide interacts with bilayers, monolayers are commonly used to study lipid surfaces in contact with trehalose solution (3–5). The applicability of these results to cell membranes relies on the equivalence of the two systems in their response to trehalose. Although a bilayer cannot simply be considered to consist of two independent monolayers (6,7), the headgroup/water interfaces in the two systems may be sufficiently similar to make monolayers effective bilayer surrogates. The responses of monolayers and bilayers to trehalose or any other substrate must therefore be compared under some of the same conditions. Although this may present difficulties experimentally, it is potentially straightforward with computer simulation.

Recent molecular dynamics (MD) simulations (8–10) of lipid bilayer/trehalose at high hydration have lent substantial insight into the interaction of trehalose and the headgroup region. In all cases trehalose intercalated into the headgroup region, formed approximately the same number of hydrogen bonds with the lipids as the water it displaced, and left the overall bilayer structure relatively unperturbed. Although these observations do not directly speak to the stabilizing effect of trehalose on bilayers at very low hydration, they are consistent with ''water replacement'' hypothesis of Crowe and co-workers (11). Given that the results were largely independent of small differences in the potential energy functions and methodologies employed, they also imply that MD can indeed be used to determine whether the responses of bilayer and monolayers to trehalose are similar.

This article compares assorted surface properties obtained from MD simulations of dipalmitoylphosphatidylcholine (DPPC) bilayers and monolayers in the presence and absence of trehalose. The primary focus is on constant area simulations at 54, 64, and 80 Å^2/lipid, 323 K, and high hydration (all over 22 waters/lipid). Although the areas other than 64 Å^2/lipid are not experimentally observed at these conditions (7), the trends can be usefully compared to those of monolayers, and the extent of correspondence can be established.

The Methods section describes the simulation systems and parameters, and construction of initial conditions. Results are presented in four subsections: general features, surface pressure-surface area isotherms, hydrogen bonding and hydration, and dipole potential and other conformational measures. Discussion and Conclusions sections follow. The Appendix presents the results from simulations at different surface tensions with and without trehalose to establish the equivalence of ensembles for this application.

METHODS

Description of systems

The 12 ''core'' bilayer and monolayer systems consisted of 80 lipids (40/leaflet), were fully hydrated (20–29 waters/lipid, as detailed in the following subsection), and contained either 0 or 40 trehalose (a 1:2 trehalose/lipid ratio). They were simulated for 20 ns each at constant particle number N, area A (54, 64, and 80 Å^2/lipid), and temperature T (323 K). The normal pressure P was set to 1 atm for bilayers, and the volume V was fixed for monolayers. Consequently, the bilayers and monolayers were simulated in the NPAT and NVT ensembles, respectively.

Results for the two other NPAT simulations are also included in the main text: 80 lipids and 160 trehalose in 6516 waters at $A = 64$ Å^2/lipid (20 ns); and 40 trehalose in 1629 waters (12 ns). The system with 160 trehalose is only used for comparison and validation here, though it will form the basis of future studies requiring a large number of trehalose. The Appendix describes NPγT simulations (where γ is surface tension) of pure DPPC and DPPC with 40 trehalose carried out at $\gamma = 10$ dyn/cm (20 ns each), 17 dyn/cm (25 ns each),

Submitted May 5, 2005, and accepted for publication September 15, 2005.
Address reprint requests to Richard W. Pastor, Tel.: 301-435-2035; E-mail: pastor@cber.fda.gov.

0006-3495/05/12/4111/11 $2.00
doi: 10.1529/biophysj.105.065953

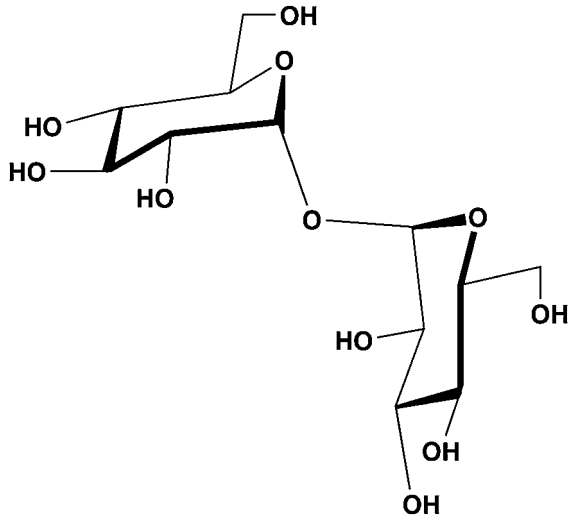

FIGURE 1 α,α-Trehalose (1,1-α-D-glucopyranosyl α-D-glucopyranoside). Henceforth, this disaccharide is simply denoted trehalose.

and 25 dyn/cm (25 ns each). Pure bilayers were also simulated at NPT (the equivalent of NPγT with $\gamma = 0$) for 10 ns, and at NPAT with $A = 60$ and 68 Å^2/lipid (15 ns each). These simulations were also carried out at 323 K.

The total time of the preceding trajectories is >400 ns.

Simulation details

Molecular dynamics simulations were performed using CHARMM (Chemistry at Harvard Macromolecular Mechanics) (12) with the C27r all-atom potential energy set for DPPC (13), CSFF for trehalose (14) and modified TIP3P for water (15,16); C27r revises the chain torsions of the older parameter C27 (17), but is otherwise identical. Newton's equations of motion were integrated using the Verlet algorithm with a 1-fs time step, and coordinates were saved every 1 ps. Simulations were carried out with periodic boundary conditions with a tetragonal lattice, with the z axis normal to the interface; i.e., the area and height vary independently while preserving the x/y ratio. Temperatures were maintained by a Hoover thermostat (18) with a coupling constant of 20,000 kcal mol^{-1} ps^{-2}, and pressures by a pressure piston (19) of mass 2000 amu. Electrostatic interactions were calculated via the particle mesh Ewald (PME) (20) method with $\kappa = 0.33$ A^{-1}, and the fast-Fourier grid densities set to ~1/Å. Lennard-Jones energies were switched to zero between 7–10 Å. SHAKE (21) was used to constrain all covalent bonds involving hydrogen atoms.

All constant area averages were evaluated from 3 to 20 ns for pure bilayers and monolayers, and for the final 10 ns for those with trehalose; those at constant surface tension were evaluated from 5 ns. These ranges were determined from inspection of time series (cf. Figs. 6 and 9), and comparisons of means from assorted intervals using t-tests (22). Statistically independent block sizes were evaluated using standard methods (23). Standard deviations over these block sizes were then used to estimate the standard error (SE) for the averages.

Surface tensions were evaluated from the relation (24):

$$\gamma = \frac{1}{2}\left\langle L_z\left(P_{zz} - \frac{1}{2}(P_{xx} + P_{yy})\right)\right\rangle, \quad (1)$$

where L_z is the length of the simulation cell normal to the bilayer surface, P_{zz} is the component of the pressure tensor normal to the bilayer surface, and P_{xx} and P_{yy} are the tangential components. The factor of 1/2 arises because there are two interfaces in the system, so the units of surface tensions reported here are understood to be dyn/cm/leaflet. The surface pressure π of the monolayer was evaluated from the calculated surface tension and

$$\pi = \gamma_0 - \gamma, \quad (2)$$

where γ_0 is the experimental surface tension of water (67.9 dyn/cm at 323 K) (25). Because of the geometry of the simulation system (two interfaces), the calculated surface pressures can be compared directly with experiment.

Because lipid monolayers were simulated at constant volume, the recently developed (26) pressure-based long-range correction was not included in any of the simulations presented here. This is expected to have a small effect of the calculated surface tensions of the bilayers, but does lead to underestimates of surface tension for liquid/vapor interfaces (26). The 8 dyn/cm underestimate for the surface tension observed in simulations of heptane/vacuum without a long-range correction provides a reasonable first approximation for the corresponding underestimate in monolayers.

Hydrogen bonds were assumed to exist when selected oxygens and hydrogens (either in the primary or image cell) were closer than 2.4 Å (27).

Waters were considered bound to the bilayer if their oxygen atoms were between $\langle z_P^l\rangle - \xi_l$ and $\langle z_P^u\rangle + \xi_u$, where $\langle z_P^l\rangle$ and $\langle z_P^u\rangle$ are the average phosphate positions of the lower ($z < 0$) and upper ($z > 0$) leaflets, respectively, at each time point; $\xi_l = 2.66 \times sd[z_P^l]$, and $sd[z_P^l]$ is the standard deviation of the phosphate distribution for the lower leaflet at the same time point (ξ_u is defined similarly). The multiplier 2.66 was chosen to yield an average value of bound water/lipid close to 9 for the bilayer at 64 Å^2/lipid and thereby reasonably corresponds with the experimental value of 8.6 (7). To allow for partial binding of an individual trehalose molecule i, a fractional binding, f_i, was computed as the number of sugar heavy atoms within the same cutoff, divided by the total (23 atoms) for each sugar. The total number of trehalose bound is defined as $\sum f_i$. Binding counts for monolayer systems were defined analogously.

The electrostatic potential drop $\Delta\Psi(z)$ across the interface arising from the nonuniform distribution of dipoles was calculated by the following double integral (28):

$$\Delta\Psi(z) = \Psi(z) - \Psi(\pm\infty) = -\frac{4\pi}{\varepsilon_0}\int_{\pm\infty}^{z} dz' \int_{\pm\infty}^{z'} \rho(z'')dz'', \quad (3)$$

where $\rho(z)$ is the time-averaged charge density from 0.2 Å bins. Bilayers and monolayers were placed in the same configuration, with the center of the water layer at $z = 0$, and the chains extending to large (or negative) z, and the integration was extended to a region of no charge. $\Delta\Psi(z)$ was also calculated separately for lipids, water, and trehalose.

Preparation of initial conditions

Minimization procedures used either the steepest descent (SD) algorithm, the adapted basis Newton Raphson (ABNR) algorithm, or usually both. Bad atom contacts are relieved with an initial short SD minimization, followed by a longer ABNR minimization, which employs an adaptive step size. In the following model building descriptions, brief minimization will be used to indicate 10–20 steps of SD followed by 50–200 steps of the ABNR algorithm, whereas extended minimization will indicate 50–100 steps of SD followed by 500–1000 steps of the ABNR algorithm. Exceptions to this convention will note the algorithm and number of steps used.

Coordinates for α,α-trehalose (α-D-glucopyranosyl α-D-glucopyranoside, compact notation [α-D-Glc$p$-(1 ↔ 1)-α-D-Glc$p$]) were obtained from Brown et al. (29), and prepared for model building by a brief minimization in vacuo.

A bilayer with surface area 64 Å^2/lipid was constructed de novo from a library of DPPC conformations extracted from a previous MD simulation (26). Analysis of the headgroup torsions from that simulation indicated some persistent model building artifacts; overpopulated conformations were culled to produce a library of 1462 conformations. Individual lipids were randomly selected from the library and placed on a hexagonal lattice in the xy plane symmetric about the z axis, with a spacing of 9.1 Å between lipids in a row and between rows. Forty lipids were placed in each leaflet, rotating by 180° for the second leaflet, with the phosphate groups at approximately ±18 Å in the z direction (the cleavage plane is at $z = 0$). A tetragonal lattice

with $A = B = 50.596$ Å and $C = 67$ Å was defined, and internal coordinate restraints of 100 kcal/mol were imposed on the lipid headgroup dihedrals. To preserve headgroup conformations, these restraints were kept in place throughout the minimizations described below. To relieve bad contacts, the placed lipids were minimized for 100 steps with the SD algorithm using only Lennard-Jones, bond, improper dihedral, and the restraint terms. The full potential was restored, and an additional 100 steps of SD minimization was performed. The SHAKE constraint was added, and 200 steps of ABNR minimization completed the initial relaxation of stress induced by model building. Next, eight preequilibrated 25.2 Å boxes of TIP3P waters were placed to create two slabs, one above and one below the bilayer, starting from the average C=O position of each leaflet and extending outward, away from the $z = 0$ plane. Waters that badly overlapped lipid atoms (centers closer than 2.2 Å) and those outside the $z = \pm 33.5$ Å dimensions of the unit cell were deleted, for a total of 2324 waters (29 per lipid). To this point, the minimizations used force-shifted spherical truncation with a 10 Å cutoff; with the addition of solvent, the electrostatic treatment was changed to PME, using the same PME options specified above for the simulations. This system was subjected to an extended minimization. The entire solvated bilayer construction process was repeated seven more times with different initial random seeds, and the resulting eight models were evaluated on their potential energies and agreement with experimental deuterium order parameters (30) and atom distributions (31,32) as described previously (33). The selected system was set up for NPAT dynamics with no restraints and heated from 223 to 323 K over 10 ps, and equilibrated for another 90 ps using velocity adjustments every picosecond via simple three-step Verlet; after 100 ps, the Hoover thermostat was added to maintain the temperature at 323 K. The system was further equilibrated for 1.2 ns, and the final coordinate set was used as the starting point for all subsequent model building and simulations.

To prepare systems at larger and smaller lipid surface areas, two separate NPγT simulations were started from the initial equilibrated model just described, using more extreme values for the surface tension. Expansion with $\gamma = 50$ dyn/cm passed through the target value of 80 Å^2 after ~1.6 ns. Compression from 64 Å^2 was carried out in four stages to reach 54 Å^2: $\gamma = 0$ dyn/cm for 500 ps; $\gamma = -10$ dyn/cm for 500 ps; $\gamma = -15$ dyn/cm for 1.1 ns; $\gamma = -25$ dyn/cm for 1.1 ns. The trajectory with $\gamma = 0$ dyn/cm was continued to illustrate the behavior of the system when simulated at NPT.

After 1 ns of further equilibration at NPAT, coordinates of the pure systems were replicated and 40 trehalose were layered ~2 Å above the positions of the phosphates. Overlapping waters were deleted to yield 1733, 1629, and 1580 waters for surface areas 54, 64, and 80 Å^2, respectively, and then each was subjected to an extended minimization. Ring restraints were applied to the sugar during minimization to prevent flipping into the high-energy twisted boat configuration, and were removed for subsequent dynamics. The temperature was set to 223 K and raised in increments of 10° over the first 100 ps until it reached 323 K.

NPγT simulations were initialized from NPAT pure lipid trajectory for 64 Å^2 at 3 ns ($\gamma = 10$ dyn/cm) and 15 ns ($\gamma = 17$ and 25 dyn/cm). The 40 trehalose were added as described above, yielding 1629 waters for $\gamma = 10$ dyn/cm and 1636 waters for $\gamma = 17$ and 25 dyn/cm.

Monolayers were constructed from the corresponding minimized bilayers at each area/lipid by inverting the layering via translation (water in the middle instead of at the ends), and extending L_z by 30–35 Å to provide a vacuum space at the chain ends (24). Specifically, based on the lipid phosphorous atoms and water oxygen atoms, molecules with negative z coordinates for these atoms were translated by L_z in the $+z$ direction, then the entire system was translated by $L_z/2$ in the $-z$ direction to recenter with respect to the $z = 0$ plane. A brief minimization was performed to relax the chain ends.

The box of 40 trehalose and 1629 waters was extracted from the 20-ns point of the NPAT simulation of the bilayer with trehalose at 64 Å^2/lipid. Due to the irregular boundary in the z dimension from the deletion of the lipids, a series of brief minimizations was employed while reducing L_z from 46 to 36 Å by 1-Å increments, and then to 32 Å by 0.25 Å for the initial slab shape. The system was simulated for 12 ns at NPAT, using the same protocol and cross-sectional area as the system from which it was extracted.

Three copies of the 12-ns coordinate set from the trehalose and water slab simulation were stacked along z and then added back to the same 20-ns coordinate set from the bilayer with trehalose, to create a bilayer system elongated in z with 160 trehalose and 6516 water molecules. A gap of 2 Å was left between the coordinates from the slab and the bilayer systems, and L_z was increased accordingly. L_z was then decreased by 0.25 Å increments to ~139.5 Å with brief minimizations, with restraints used to maintain the shapes of the trehalose molecules. The resulting system of 37,148 atoms was then simulated for 20 ns with the same NPAT protocol as above.

RESULTS

General features

Figs. 2 and 3 show the 20-ns snapshots of bilayer and monolayer simulations with trehalose at an area per lipid of 64 Å^2. Although some of the trehalose clearly interacts with the bilayer, a substantial fraction remains in solution. Fig. 4 compares the total electron densities of these two systems, a solution containing the same number of trehalose and water (1.363 molal), the bilayer at 64 Å^2/lipid containing four times as many trehalose and water (included here for validation purposes), and the bilayer and monolayer at 80 Å^2/lipid (the systems with the smallest water/trehalose layer). The densities in the headgroup regions of the bilayer and monolayer pairs are nearly identical (differences in the chains are differed to the Discussion). The density of the trehalose/water solution is 1.0964 ± 0.0003 g/cc, which compares well with the experimental value of 1.126 g/cc (34). Importantly, the densities of all systems near the center of the water layer ($z = 0$) are the same. This indicates that the bilayers and monolayers

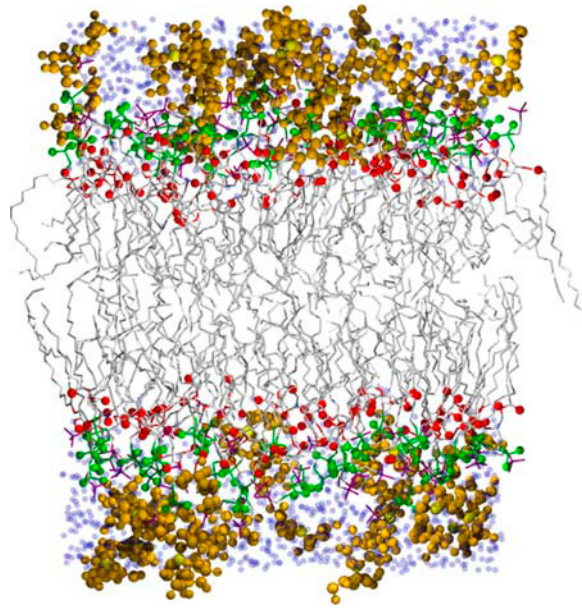

FIGURE 2 DPPC bilayer with 40 trehalose from the 20-ns point of NPAT simulation at 64 Å^2/lipid. Coloring is as follows: glycosidic oxygen of trehalose, yellow; all other trehalose atoms, orange; phosphate groups of DPPC, green; $N(CH_3)_3$, purple; carbonyl oxygen, red; all other lipid atoms, gray; waters, transparent blue.

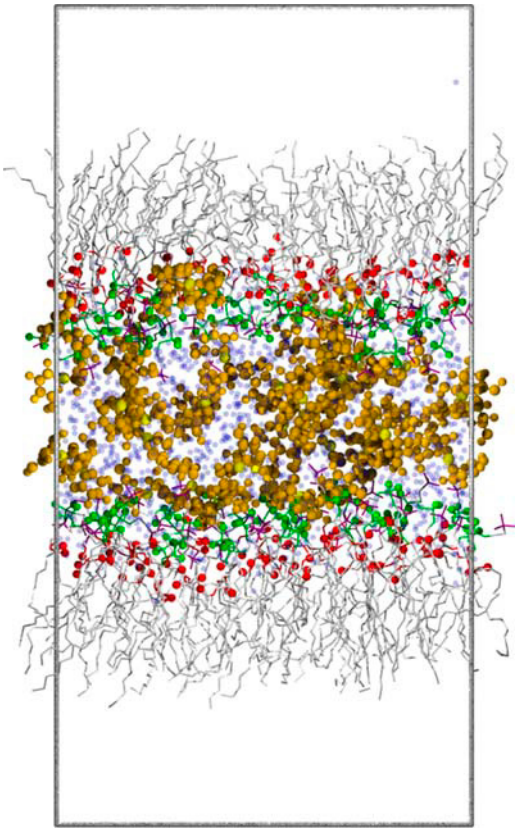

FIGURE 3 DPPC monolayer with 40 trehalose from the 20-ns point from the trajectory at 64 Å^2/lipid. Heavy lines indicate the boundaries of the simulation cell, which includes a vacuum/chain interface. Atom coloring is as for Fig. 2.

simulated here are sufficiently large to allow a trehalose ''solution'' between leaflets, and that potential artifacts associated with small system size are unlikely to confound the assorted comparisons to follow.

Fig. 5 compares the electron densities of trehalose, water, phosphate, and carbonyl for the bilayer and monolayer at 64 Å^2/lipid. Partitioning of trehalose into the bilayer and monolayer is qualitatively similar, with the trehalose substantially overlapping the phosphate distribution, but not all of the carbonyl. The apparent shoulders in the trehalose distribution in the bilayer are not evident in the monolayer, although, as shown below, this difference does not affect the other averages to within statistical error. Based on the degree of symmetry of the distributions in opposing leaflets, the simulation of the bilayer is better converged than that of the monolayer. The simulations at 54 Å^2/lipid are the least converged of the three areas because the high packing density restricts motion.

Surface pressure-surface area isotherms

Fig. 6 plots the 1-ns block averages of the surface tensions for the systems at 64 Å^2/lipid; the average surface tensions and average SE for all three surface areas are listed in the first block of data in Table 1. Even though the fluctuations

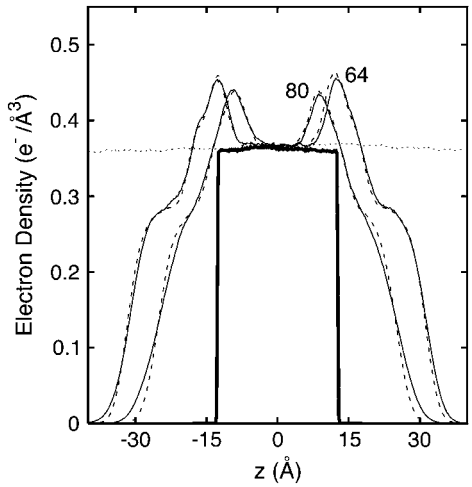

FIGURE 4 Total density distribution for bilayers (*solid curves*) and monolayers (*dashed curves*) with 40 trehalose, the water/trehalose region of the bilayer with 160 trehalose and 6516 water (*dotted curve*), and a solution of 40 trehalose and 1629 water (*thick solid curve*). For this and related plots the bilayer and monolayer are placed in same orientation; i.e., with the water in the center ($z = 0$) and the chains extended toward vacuum for the monolayers and toward the other leaflet for the bilayer. The bilayer midplane (the position of the methyl through) is at $z = \pm 32.95$ Å.

shown in Fig. 6 are large, the SE of the mean surface tensions are in the 1–2 dyn/cm range. This precision is sufficient for this study.

Fig. 7 compares surface pressures of pure monolayers (calculated from Eq. 2 and the surface tensions listed in Table 1) and experiment (35,36). The excellent agreement provides an important validation. Although there is likely some cancellation of errors (see Methods), because this study focuses on changes in surface tension upon addition of trehalose, it is reasonable to expect that such errors will continue to cancel.

From Table 1 and Fig. 8, trehalose lowers the surface tension (raises the surface pressure) of bilayers and monolayers approximately the same amount at each surface area, even though the total surface tensions are quite different. The surface tension differences are statistically significant ($p < 0.05$) for all systems, as ascertained by *t*-tests over 1- and 2-ns block averages. The values of $\Delta\gamma$ are also independent of surface area, within the precision of the averages.

Hydrogen bonding and hydration

The second block of data in Table 1 summarizes hydrogen bond (H-bond) counts to the carbonyl and phosphate groups of DPPC by water and trehalose. Several trends are evident: 1), H-bonding increases as surface area increases, as would be expected given the increasing exposure to solvent. 2), Results for bilayers and monolayers are typically within 1–2 SE of each other for each surface area, again indicating the correspondence of these two systems. 3), The number of H-bonds to water decreases when trehalose is added.

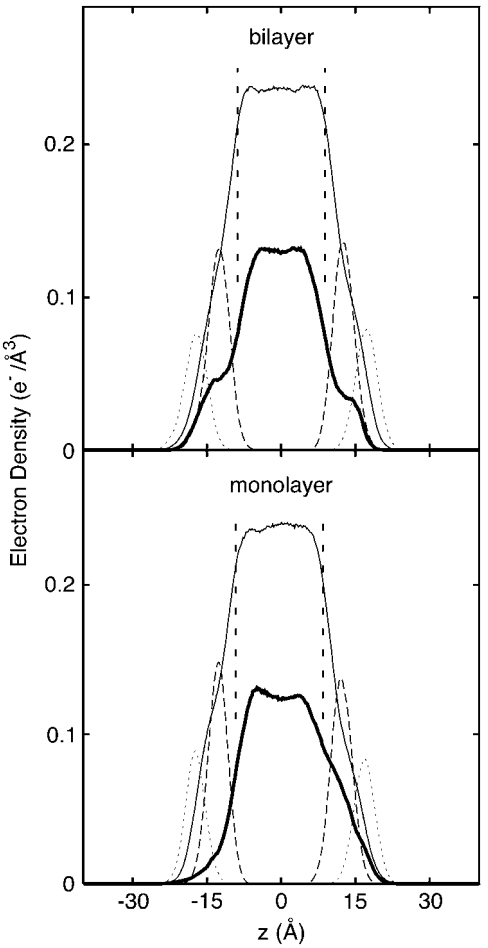

FIGURE 5 Electron density distribution of trehalose (*thick solid curve*), water (*solid curve*), phosphate (*dashed curve*), and carbonyl (*dotted curve*) group from simulations of the bilayer (*top*) and monolayer (*bottom*) at 64 Å^2/lipid. The dashed vertical lines at $z \approx \pm 9$ Å show the average cutoffs used for trehalose and water counting (see Methods).

4), Trehalose forms H-bonds to both the carbonyl and phosphate groups. 5), The total number of solvent/headgroup H-bonds is only slightly smaller in systems with trehalose; i.e., trehalose appears to be an effective surrogate for water, at least in terms of hydrogen bond stabilization to the lipids.

There is a substantial amount of water in the headgroup region that is not directly involved in hydrogen bonds with the lipids. Fig. 9 shows the time series of water and trehalose counts for $A = 64$ Å^2/lipid systems. Averages for all the surface areas are listed in the third block of data in Table 1. Some of the trends are similar to that observed for H-bonds: water and trehalose occupancies are proportional to surface area, and the results for bilayers and monolayers are largely comparable. Of note is the large number of waters that trehalose displaces. To use a specific example, the hydration is decreased by 1.8 waters/lipid, or 144 waters for the bilayer at $A = 64$ Å^2/lipid. This implies that the 10.3 bound trehalose have displaced an average of 14 waters each.

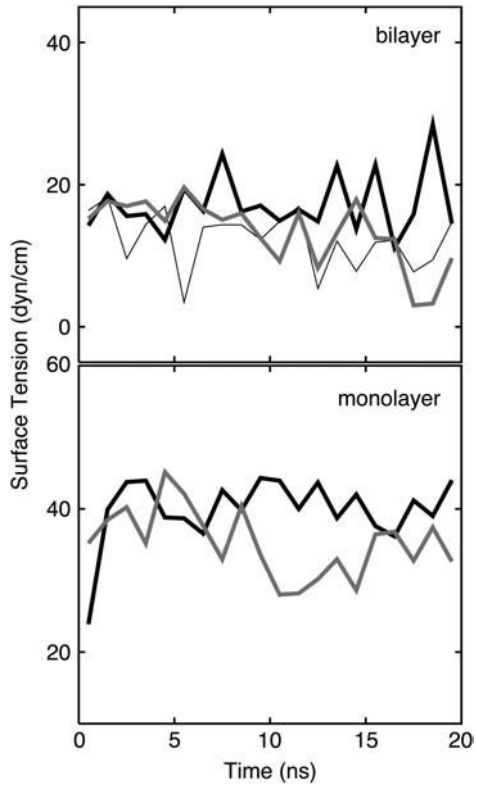

FIGURE 6 Time series (1-ns block averages) of surface tension at $A = 64$ Å^2/lipid for the bilayers (*top*) and monolayers (*bottom*) of pure DPPC (*thick black line*), with 40 trehalose (*thick gray line*), and 160 trehalose (*thin black line*).

Dipole potential and other conformational measures

Fig. 10 plots the dipole potential $\Delta\Psi$ for systems at $A = 64$ Å^2/lipid, with the pure systems and those with trehalose on opposite sides for easy comparison. Values of $\Delta\Delta\Psi$ are listed in the last block of entries in Table 1. Beginning with the pure systems, the total potential drop is a difference in a large positive contribution from the lipids and a large negative one from the water. These individual components as well as the total are almost identical for the bilayer and monolayer. Trehalose reduces the contribution of the water (as expected from the depletion of water in the headgroup region), and contributes a negative term of its own. The positive contribution of the lipids is also reduced (indicating some conformational rearrangement), and the net result is a small reduction in magnitude of the potential with respect to the pure systems; i.e., $\Delta\Delta\Psi = 50$ mV. Similar results are obtained at the other areas (Table 1). The average statistical errors are relatively large, especially for the lipid components. However, the similarity of signs in the assorted components of $\Delta\Delta\Psi$ across bilayers, monolayers, and areas supports statistical significance.

A number of other conformational properties of the lipids were evaluated, including deuterium order parameters of the chains and the headgroup, and angles of PN and C=O vectors

TABLE 1 Averages for properties described in the text, with differences Δ taken to be system with trehalose minus pure DPPC

		54 Å^2/lipid		64 Å^2/lipid		80 Å^2/lipid		
Property	Atoms; system	Bi	Mono	Bi	Mono	Bi	Mono	Average SE
surface tension (dyn/cm)	Pure DPPC	1.2	17.1	17.5	40.7	23.9	53.5	1.0
	+Trehalose	−4.0	11.7	10.5	32.4	19.5	48.1	1.7
	Δ γ	−5.2	−5.4	−7.0	−8.3	−4.4	−5.4	1.9
H-bonds (per lipid)	CO-water; pure	0.94	0.91	1.24	1.22	1.50	1.48	0.01
	CO-water; +trehalose	0.82	0.90	1.09	1.07	1.32	1.24	0.01
	CO-trehalose	0.02	0.01	0.07	0.07	0.12	0.12	0.00
	CO total; +trehalose	0.84	0.91	1.16	1.14	1.44	1.36	0.02
	Δ CO total	−0.11	0.00	−0.08	−0.08	−0.06	−0.12	0.03
	PO_4-water; pure	3.94	3.95	4.19	4.13	4.37	4.36	0.01
	PO_4-water; +trehalose	3.58	3.57	3.63	3.57	3.74	3.69	0.02
	PO_4-trehalose	0.32	0.32	0.44	0.53	0.56	0.56	0.02
	PO_4 total; +trehalose	3.90	3.90	4.07	4.09	4.30	4.25	0.04
	Δ PO_4 total	−0.04	−0.05	−0.12	−0.04	−0.07	−0.11	0.04
Occupancy (counts)	Water; pure	6.0	6.0	8.9	8.3	12.6	12.4	0.1
	Δ Water/lipid	−0.6	−0.6	−1.8	−1.6	−2.6	−2.5	0.2
	Trehalose	4.2	4.6	10.3	10.6	19.2	19.4	0.4
	Δ Water/trehalose	12	10	14	12	11	10	2
ΔΔΨ (mV)	Lipid	90	−30	−200	−290	−130	−120	90
	Water	310	400	530	610	510	450	110
	Trehalose	−290	−320	−280	−270	−260	−250	10
	Total	110	50	50	50	120	80	40

The average SE in the final column is estimated from the standard errors obtained for entries in the same row.

with respect to the bilayer normal. Differences between systems with and without trehalose and between bilayers and monolayers were all within statistical error at each surface, and are not reported. Consequently, although changes in the bilayer structure were evidenced by the lipid component of the dipole potential, these changes are quite small.

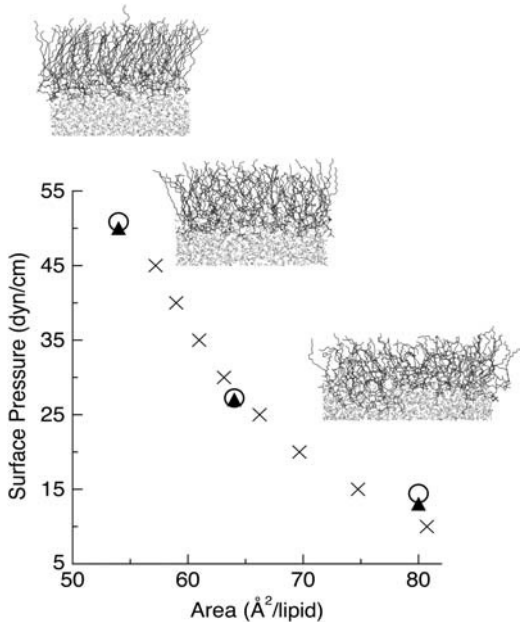

FIGURE 7 Comparison of simulated (○) and experimental surface pressure versus surface area (π-A) isotherms for pure DPPC monolayers. Experimental data at 323 K (×) and 321 K (▲) are from references 35 and 36, respectively. Images of the 20-ns trajectory point for one leaflet of each simulated system are included, with areas 54, 64, and 80 Å^2/lipid from left to right.

DISCUSSION

The essential result of this study is that the response of bilayers and monolayers to trehalose is virtually equivalent at the concentration simulated (~1.4 molal, 1 trehalose/2

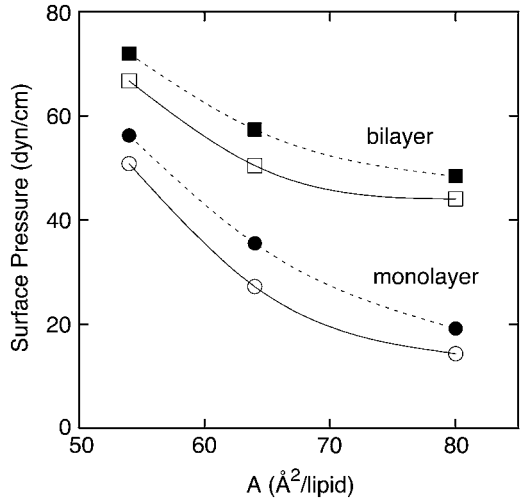

FIGURE 8 π-A isotherms at 323 K for DPPC monolayers (*circles*) and bilayers (*squares*). Pure systems in open symbols; those with 40 trehalose (a 1:2 trehalose/lipid ratio) in solid symbols. SE is comparable to the size of the symbols; lines are included to guide the eye.

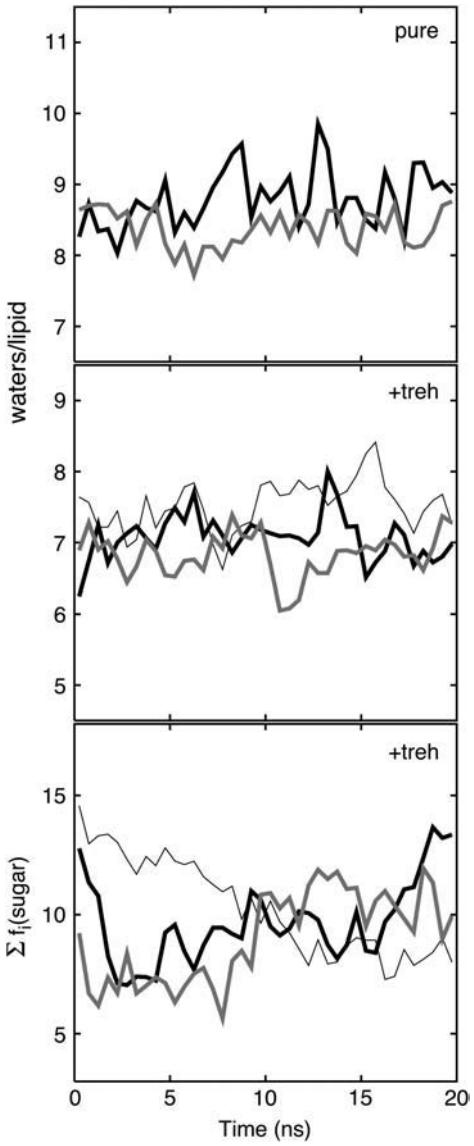

FIGURE 9 Time series (500-ps block averages) of water and trehalose binding based on the dividing surface described in Methods and illustrated in Fig. 5. Bilayer (*thick black line*), monolayer (*thick gray line*), and 160 trehalose (*thin black line*) systems are shown at $A = 64$ Å^2/lipid.

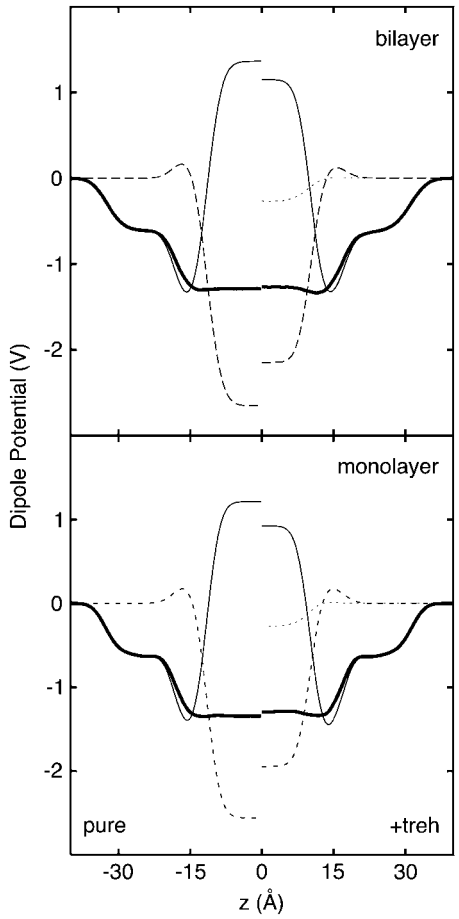

FIGURE 10 Dipole potential for lipids (*solid curves*), water (*dashed curves*), trehalose (*dotted curve*), and total (*thick solid curves*). The center of the water layer is at $z = 0$ for both bilayers and monolayers.

DPPC). Although this observation is most relevant for bilayers near the experimental surface area (64 Å^2/lipid for DPPC), the correspondence at the extreme areas of 54 and 80 Å^2/lipid supports obtaining data at a wide range of monolayer surface areas for additional insight. The quantities reported here, surface tension (or surface pressure), hydrogen bonding, hydration, and dipole potential, and now considered in more detail, and related to results from experiment and other recent simulations of bilayer/trehalose systems when possible.

First, the pure monolayer π-A isotherm (Fig. 7) agrees very well with experiment, though additional testing is required to determine whether this result is fortuitous. The increase in surface pressure upon addition of trehalose (Fig. 8) is qualitatively similar to that observed in fluid phase monolayers of dimyristoyl phosphatidylcholine at 303 K (3). A more quantitative comparison is not possible because the effective concentration of trehalose at the lipid/water interface is not known. The effect of trehalose on monolayer surface pressure below the phase transition temperature varies substantially with surface area (37), so the trend observed here is significant.

The discussion of the bilayer surface tensions requires a preamble. DPPC bilayers of 36–40 lipids/leaflet near the experimental surface area per lipid have surface tensions near 20 dyn/cm when simulated with the CHARMM force field C27r. This result is controversial because the experimentally determined surface tension of macroscopic nonstressed lipid bilayers is close to or equal to zero (38). Feller and Pastor (39) proposed that $\gamma \neq 0$ for simulation sized bilayers because long-wavelength undulations are not present. Consequently a nonzero surface tension must be applied in NPγT simulations in what may be regarded as a small system correction. The Appendix provides examples of NPγT simulations, including $\gamma = 0$ (the equivalent of NPT).

Others (38,40–43) have argued that the nonzero surface tension observed in simulations is an artifact for the force field; i.e., a correctly parameterized set should yield $\gamma = 0$ dyn/cm for a nonstressed lipid bilayer at the correct surface area. Some force fields, including the one used by Sum et al. (8) for their simulation of DPPC and trehalose, do in fact have this property. Ultimately, extensive and systematic comparisons of bilayer and monolayer properties with experiment, and simulations on larger systems will be required to resolve this question. For here it is reasonable to focus on the relative surface tensions of the systems simulated.

First, bilayers show the same trend as monolayers of increasing surface tension (decreasing surface pressure) with increasing surface area, although the slopes and surface tensions are higher for the monolayers (Fig. 8 and Table 1). The curvature is related to the compressibility modulus K_a, which is defined as follows

$$K_a = A\left(\frac{d\gamma}{dA}\right)_T = -A\left(\frac{d\pi}{dA}\right)_T. \quad (4)$$

Although additional intermediate points are needed for a quantitative comparison, these results suggest that K_a of a bilayer leaflet is smaller than that of a monolayer. Nevertheless, the 4–8 dyn/cm drop in surface tension upon addition of trehalose is statistically equivalent at each area simulated. This implies that the headgroup/water interfaces of the two systems are very similar.

The equivalence of the response to trehalose and marked differences for γ and K_a in bilayers and monolayers implicate the chains. As illustrated in Fig. 11, the chains from the bilayer leaflets are more extended than those from the monolayer, and mix with the those in the opposing leaflet. This observation was anticipated by Nagle (6), who proposed that mixing couples the leaflets, and argued that a bilayer cannot simply be treated as two monolayers. Recent simulations have indicated that the tangential pressure P_T in the bilayer center is positive, leading to a negative surface tension in this region (40,41,44). In contrast, the monolayer chains are in contact with vacuum in this simulation (air in experiment). They are flatter, and, like an alkane/air interface, have a positive surface tension. These considerations qualitatively explain the observed 15–30 dyn/cm differences in surface tensions already noted. The total surface tension contains contributions from the headgroup and chain regions. Assuming that the headgroup/water surface tensions are the same at each area, the chain/chain interactions then lower the total surface tension for bilayers whereas the chain/air interactions raise it for monolayers.

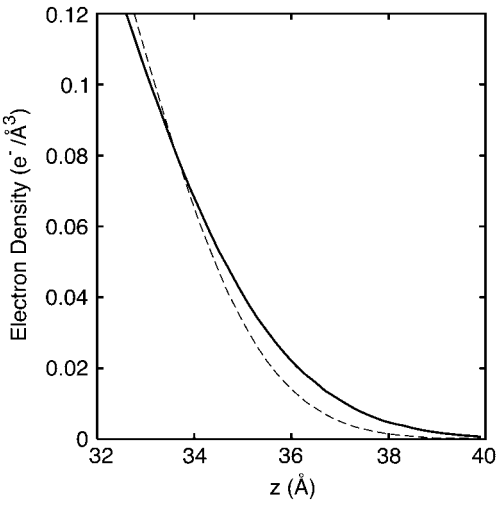

FIGURE 11 Detail from Fig. 4 of the chain methyl regions of the bilayer (*solid line*) and monolayer (*dashed line*). The bilayer midplane is at $z = \pm 32.95$ Å.

Results for location of trehalose in bilayer, hydrogen bonding to the headgroup, water occupancy, and bilayer stability are very similar to the those obtained in recent MD studies of trehalose/bilayer systems at high hydration (8–10), even though somewhat different conditions, force fields, and methods were applied. Some trehalose intercalates deeply into the headgroup region and interacts with the carbonyl groups, in agreement with Fourier transform infrared spectroscopy measurements (5), whereas others only associate with the phosphates (Figs. 2, 3, and 5). Trehalose essentially displaces the number of waters expected from its molar volume and replaces close to all of the hydrogen bonds to the headgroup previously made to these waters (Fig. 9 and Table 1). This is accomplished with minimum perturbation to the overall structure, as evaluated by deuterium order parameters, and PN and C=O orientation.

Trehalose led to a 50–100 mV drop in the magnitude of the dipole potential (Fig. 10 and Table 1), which agrees with results on liquid expanded dimyristoylphosphatidylcholine monolayers (4,5). This quantity appears to be extremely sensitive to small changes in lipid orientation, and the total change is the difference in large contributions from the water, lipids, and trehalose itself. It is likely that the surface tension reduction is related to the drop in the dipole potential. The simulations of Villarreal et al. (10) also revealed a reduction in the magnitude of dipole potential, though smaller than reported here. Given the fact that $\Delta\Psi$is the sum of several contributions of opposite sign, it is not surprising that it is sensitive to simulation details.

CONCLUSIONS

The principal conclusion of this study is that under conditions of full hydration and a 1:2 trehalose/lipid ratio, trehalose perturbs the surfaces of bilayers and monolayers in the same way. It lowers the surface tension (raises the surface pressure), displaces water from the headgroup region, mostly replaces hydrogen bonds to the headgroup made by the water, and slightly reduces the magnitude of the potential drop. The chain regions of the systems are essentially unperturbed by trehalose.

The headgroup regions of the pure bilayers and monolayers are also remarkably similar in terms of water occupancy and hydrogen bonds, and dipole potential. In contrast, the chain/chain interface of bilayers is quite different from the chain/air interface of monolayers. This qualitatively explains the differences in local surface tensions of these two systems, and limits their correspondence. Furthermore, undulations of bilayers on the macroscopic length scale contrast the flatness of monolayers.

This and other recent simulations of trehalose/bilayer systems were at high hydration, and therefore do not directly probe the very dry states where trehalose acts as a preservative. Nevertheless, the results are consistent with membrane preservation by trehalose, in that waters are replaced whereas the overall bilayer structure is almost unperturbed. Additionally, the similarity of results obtained from different force fields and methods lends confidence that MD simulations can be fruitfully applied to the low hydration regime.

APPENDIX: EQUIVALENCE OF CONSTANT AREA AND CONSTANT SURFACE TENSION ENSEMBLES

Constant pressure and temperature ensembles are used to allow the dimensions of the system to adjust because the initial condition is not clearly known, or because volume or area fluctuations are of interest. These ensembles include the NPAT already described in the text, and NPγT, where γ is the applied surface tension (24). When $\gamma = 0$, NPγT reverts to the well-known NPT ensemble (23). Averages calculated from these ensembles are expected to be identical for very large systems, though may differ when the system is ''small''. Whereas current MD simulations of lipid bilayers contain many thousands of particles, the number of lipids is typically ~50 per leaflet. Consequently, it is not always clear whether the large-system limit has been reached for a particular application. Systems with membrane active components are of special concern: intercalation into the bilayer may be very different in NPγT and NPAT ensembles because of fluctuations in the total surface area in the former. Fortunately, there is a straightforward test for equivalence: if simulations carried out at constant areas reveal lowering of surface tension upon the addition of trehalose, an increase in the surface area should be observed when the same systems are simulated at constant surface tensions. Put another way, the γ-A isotherms for the two ensembles should be consistent.

From the calculated surface tensions listed in Table 1 for pure DPPC bilayers, NPγT simulations carried out at applied surface tensions of 10, 17, and 25 dyn/cm should yield average area/lipid $\langle A \rangle$ of 60, 64, and 80 Å^2 if the NPAT and NPγT ensembles are equivalent. The addition of trehalose reduces the bilayer surface tension by 4–8 dyn/cm. This implies, for example, that an applied surface tension of 17 dyn/cm should increase $\langle A \rangle$ to a value >64 Å^2 upon addition of trehalose, because the stretching force arising from the applied surface tension is larger than the contracting force of the intrinsic surface tension. The system should expand to an area where these forces are equal, as consistent with the γ-A isotherm.

Fig. 12 plots the surface areas for NPγT simulations of pure DPPC and DPPC with trehalose, starting from 64 Å^2/lipid. For notational simplicity, the units dyn/cm for applied surface tension are henceforth omitted. Qualitatively, the systems behave as expected: the pure bilayers contract to $\langle A \rangle = 59.7 \pm 0.3$ when $\gamma = 10$, expand to $\langle A \rangle = 81.8 \pm 1.5$ when $\gamma = 25$, and remain relatively close to 64 Å^2 when $\gamma = 17$ ($\langle A \rangle = 67.0 \pm 1.9$). The systems with trehalose increased to $\langle A \rangle = 70.7 \pm 0.9$ for $\gamma = 17$, and to well over 95 for $\gamma = 25$ (this system has not yet converged), though are similar for $\gamma = 10$ ($\langle A \rangle = 59.5 \pm 0.5$).

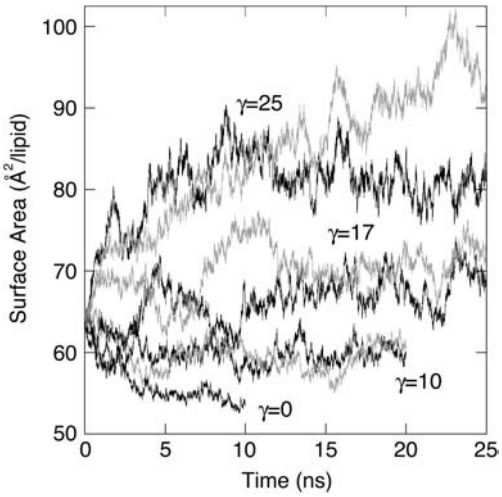

FIGURE 12 Trajectories of NPγT simulations of pure bilayers (*black lines*) and bilayers with trehalose (*gray lines*) at applied surface tensions of 0, 10, 17, and 25 dyn/cm. Points are 5-ps averages.

Fig. 13 plots the γ-$\langle A \rangle$ points from both the NPγT and the NPAT simulations. The area from the simulation with trehalose at $\gamma = 25$ is not included because it did not converge to a stable surface area (Fig. 12). Within statistical error, points from the two ensembles lie on the same isotherms. This supports the assertion that the ensembles are equivalent for

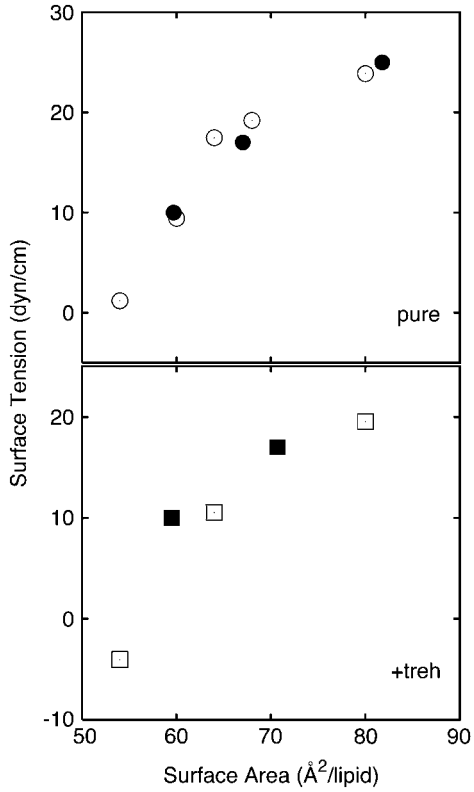

FIGURE 13 Surface tension-surface area isotherms at 323 K for pure DPPC (*top*, *circles*) and DPPC with 40 trehalose (*bottom*, *squares*). Simulations carried out at NPAT in open symbols; those at NPγT in solid symbols. SE is comparable to the size of the symbols.

the present systems. Because the large system limit for bilayers will be different for different solutes and different applications, it is reasonable to carry out preliminary studies in several ensembles.

When pure DPPC bilayers are simulated with CHARMM parameter sets C27r and $\gamma = 0$ with tetragonal boundary conditions, the surface area shrinks dramatically. This is illustrated in Fig. 12, where after several nanoseconds the surface area/lipid approaches values observed for the gel phase (47.9 $Å^2$ at 293 K). The preceding results are similar to those observed for NPT simulations of pure DPPC bilayers with earlier CHARMM parameters (45,46) and GROMOS96 45A3 (47). The reason for the contraction is as follows. The surface tension of pure DPPC at an area of 64 $Å^2$ is 17 dyn/cm for C27r (Table 1). A positive surface tension implies that the tangential pressure P_T is negative when the normal pressure P_N is 1 atm (Eq. 1). Consequently, the system contracts in the absence of a counterbalancing positive applied surface tension.

As a final technical point, the large contraction at $\gamma = 0$ is only observed when the pressure scaling is anisotropic; i.e., the area of the simulation cell can fluctuate independently of its height. A reduction in area is accompanied by an increase in height, thereby maintaining the volume approximately constant. If pressure scaling is isotropic (a single scaling is applied to each cell dimension), any reduction in area is coupled with a reduction in height and thereby a decrease in volume. This is energetically unfavorable, and will prevent any substantial contraction in area.

We thank John Brady, Bernard Brooks, Attilo Cesaro, Stephen Hall, Jeffrey Klauda, John Nagle, Lennart Nilsson, and Russell Negin for helpful discussions and technical advice. This study utilized the high-performance computational capabilities of the CIT Biowulf/LoBoS3 and NHLBI LoBoS clusters at the National Institutes of Health, Bethesda, MD.

REFERENCES

1. Wolkers, W. F., N. J. Walker, Y. Tamari, F. Tablin, and J. H. Crowe. 2003. Towards a clinical application of freeze-dried human platelets. *Cell Preservation Technology*. 1:175–188.
2. Karger. Basel. 1992. Biological Product Freeze-Drying and Formulation, Developments in Biological Standardization, Vol. 74. J. C. May and F. Brown, editors. S. Karger Publishers, Basel, Switzerland.
3. Crowe, J. H., M. A. Whittam, D. Chapman, and L. M. Crowe. 1984. Interactions of phospholipid monolayers with carbohydrates. *Biochim. Biophys. Acta*. 769:151–159.
4. Diaz, S., F. Lairión, J. Arroyo, A. C. Biondi de Lopez, and E. A. Disalvo. 2001. Contribution of phosphate groups to the dipole potential of dimyristoylphosphatidycholine membranes. *Langmuir*. 17:852–855.
5. Luzardo, M. del C., F. Amalfa, A. M. Nũnez, S. Díaz, A. C. Biondi de Lopez, and E. A. Disalvo. 2000. Effect of trehalose and sucrose on the hydration and dipole potential of lipid bilayers. *Biophys. J*. 78:2452–2458.
6. Nagle, J. F. 1986. Theory of lipid monolayer and bilayer chain-melting phase transitions. *Faraday Discuss. Chem. Soc*. 81:151–162.
7. Nagle, J. F., and S. Tristram-Nagle. 2000. Structure of lipid bilayers. *Biochim. Biphys. Acta*. 1469:159–195.
8. Sum, A. K., R. Faller, and J. J. de Pablo. 2003. Molecular simulation study of phospholipid bilayers and insights of the interactions with disaccharides. *Biophys. J*. 85:2830–2844.
9. Pereira, C. S., R. D. Lins, I. Chandrasekhar, L. C. Freitas, and P. H. Hünenberger. 2004. Interaction of the disaccharide trehalose with a phospholipid bilayer: a molecular dynamics study. *Biophys. J*. 85:2273–2285.
10. Villarreal, M. A., S. B. Díaz, E. A. Disalvo, and G. G. Montich. 2004. Molecular dynamics simulation study of the interaction of trehalose with lipid membranes. *Langmuir*. 20:7844–7851.
11. Crowe, J. H., L. M. Crowe, and D. Chapman. 1984. Preservation of membranes in any hydrobiotic organisms. *Science*. 223:701–703.
12. Brooks, B. R., R. E. Bruccoleri, B. D. Olafson, D. J. States, S. Swaminathan, and M. Karplus. 1983. CHARMM: a program for macromolecular energy, minimization, and dynamics calculations. *J. Comput. Chem*. 4:187–217.
13. Klauda, J. B., B. R. Brooks, A. D. MacKerell, Jr., R. M. Venable, and R. W. Pastor. 2005. An ab initio study on the torsional surface of alkanes and its effect on molecular simulations of alkanes and a DPPC bilayer. *J. Phys. Chem. B*. 109:5300–5311.
14. Kuttel, M., J. W. Brady, and K. J. Naidoo. 2002. Carbohydrate solution simulations: producing a force field with experimentally consistent primary alcohol rotational frequencies and populations. *J. Comput. Chem*. 23:1236–1243.
15. Jorgensen, W. L., J. Chandrasekhar, J. D. Madura, R. W. Impey, and M. L. Klein. 1983. Comparison of simple potential functions for simulating liquid water. *J. Chem. Phys*. 79:926–935.
16. Durell, S. R., B. R. Brooks, and A. Ben-Naim. 1994. Solvent-induced forces between 2 hydrophillic groups. *J. Phys. Chem*. 98: 2198–2202.
17. Feller, S. E., and A. D. MacKerell. 2000. An improved empirical potential energy function for molecular simulations of phospholipids. *J. Phys. Chem. B*. 104:7510–7515.
18. Hoover, W. G. 1985. Canonical dynamics: equilibrium phase-space distributions. *Phys. Rev. A*. 31:1695–1697.
19. Nosé, S., and M. L. Klein. 1983. Constant pressure molecular dynamics for molecular systems. *Mol. Phys*. 50:1055–1076.
20. Essmann, U., L. Perera, M. L. Berkowitz, T. Darden, H. Lee, and L. G. Pedersen. 1995. A smooth particle mesh Ewald method. *J. Chem. Phys*. 103:8577–8593.
21. Ryckaert, W. E., G. Ciccotti, and H. J. C. Berendsen. 1977. Numerical integration of the Cartesian equations of motion of a system with constraints: molecular dynamics of n-alkanes. *J. Comput. Phys*. 23: 327–341.
22. DeGroot, M. H. 1975. Probability and Statistics. Addison-Wesley, Reading, MA.
23. Allen, M. P., and D. J. Tildesley. 1987. Computer Simulation of Liquids. Clarendon, Oxford, UK.
24. Zhang, Y., S. E. Feller, B. R. Brooks, and R. W. Pastor. 1995. Computer simulation of liquid/liquid interfaces. I. Theory and application to octane/water. *J. Chem. Phys*. 103:10252–10266.
25. Weast, R. C. 1977. Handbook of Chemistry and Physics. A Ready-Reference Book of Chemical and Physical Data, 57th Ed. Robert C. Weast, editor. CRC Press, Cleveland, OH.
26. Lagüe, P., R. W. Pastor, and B. R. Brooks. 2004. Pressure-based long-range correction for Lennard-Jones interactions in molecular dynamics simulations: application to alkanes and interfaces. *J. Phys. Chem. B*. 108:363–368.
27. DeLoof, H., L. Nilsson, and R. Rigler. 1992. Molecular dynamics simulation of galanin in aqueous and nonaqueous solution. *J. Am. Chem. Soc*. 114:4028–4035.
28. Feller, S. E., R. W. Pastor, A. Rojnuckarin, S. Bogusz, and B. R. Brooks. 1996. The effect of electrostatic force truncation on interfacial and transport properties of water. *J. Phys. Chem*. 100:17011–17020.
29. Brown, G. M., D. C. Rohrer, B. Berking, C. A. Beevers, R. O. Gould, and R. Simpson. 1972. Crystal structure of alpha,alpha-trehalose dihydrate from 3 independent x-ray determinations. *Acta Crystallogr. B*. 28:3134–3158.
30. Seelig, A., and J. Seelig. 1974. The dynamic structure of fatty acyl chains in a phospholipid bilayer measured by deuterium magnetic resonance. *Biochemistry*. 13:4839–4845.
31. Büldt, G., H. U. Gally, J. Seelig, and G. Zaccai. 1979. Neutron diffraction studies on phosphatidylcholine model membranes. I. Head group conformation. *J. Mol. Biol*. 134:673–691.
32. Zaccai, G., G. Büldt, A. Seelig, and J. Seelig. 1979. Neutron diffraction studies on phosphatidylcholine model membranes. II. Chain conformation and segmental disorder. *J. Mol. Biol*. 134:693–706.

33. Pastor, R. W., and R. M. Venable. 1993. Molecular and stochastic dynamics simulation of lipid membranes. *In* Computer Simulation of Biomolecular Systems: Theoretical and Experimental Applications. W. F. van Gunsteren, P. K. Weiner, and A. K. Wilkinson, editors. ESCOM Science Publishers, Leiden, The Netherlands. 443–463.

34. Elias, M. E., and A. M. Elias. 1999. Trehalose + water fragile system: properties and glass transition. *J. Mol. Liquids.* 83:303–310.

35. Crane, J., G. G. Putz, and S. Hall. 1999. Persistence of phase coexistence in disaturated phosphatidylcholine monolayers at high surface pressures. *Biophys. J.* 77:3134–3143.

36. Somerharju, P. J., J. A. Virtanen, K. K. Eklund, P. Vainio, and P. K. J. Kinnuenen. 1985. 1-palmitoyl-2-pyrenedecanoyl glycerophospholipids as membrane probes: evidence for regular distribution in liquid-crystalline phosphatidylcholine bilayers. *Biochemistry.* 24:2773–2781.

37. Lambruschini, C., A. Relini, A. Ridi, L. Cordone, and A. Gliozzi. 2000. Trehalose interacts with phospholipids polar head groups in Langmuir monolayers. *Langmuir.* 16:5467–5470.

38. Jähnig, F. 1996. What is the surface tension of a lipid bilayer membrane? *Biophys. J.* 71:1348–1349.

39. Feller, S. E., and R. W. Pastor. 1996. On simulating lipid bilayers with applied surface tension: periodic boundary conditions and undulations. *Biophys. J.* 71:1350–1355.

40. Lindahl, E., and O. Edholm. 2000. Spatial and energetic-entropic decomposition of surface tension in lipid bilayers from molecular dynamics simulations. *J. Chem. Phys.* 113:3882–3893.

41. Marrink, S. J., and A. E. Mark. 2001. Effect of undulations on surface tension in simulated membranes. *J. Phys. Chem. B.* 105:6122–6127.

42. Benz, R. W., F. Castro-Roman, D. J. Tobias, and S. H. White. 2005. Experimental validation of molecular dynamics simulations of lipid bilayers: a new approach. *Biophys. J.* 88:805–817.

43. Sonne, J., F. Y. Hansen, and G. H. Peters. 2005. Methodological problems in pressure profile calculations for lipid bilayers. *J. Chem. Phys.* 122:124903–124911.

44. Gullingsrud, J., and K. Schulten. 2004. Lipid bilayer pressure profiles and mechanosensitive channel gating. *Biophys. J.* 86:3496–3509.

45. Feller, S. E., Y. Zhang, and R. W. Pastor. 1995. Computer simulation of liquid/liquid interfaces. II. Surface tension-area dependence of a bilayer and monolayer. *J. Chem. Phys.* 103:10267–10276.

46. Feller, S. E., and R. W. Pastor. 1999. Constant surface tension simulations of lipid bilayers: the sensitivity of surface areas and compressibilities. *J. Chem. Phys.* 111:1281–1287.

47. Chandrasekhar, I., D. Bakowies, A. Glättli, P. Hünenberger, C. Pereira, and W. F. van Gunsteren. 2005. Molecular dynamics simulations of lipid bilayers with GROMOS96: application of surface tension. *Mol. Sim.* 31:543–548.